arXiv:1605.01427v1 [cond-mat.str-el] 4 May 2016

# Drive Dependence of the Skyrmion Hall Effect in Disordered Systems

C. Reichhardt and C. J. Olson Reichhardt
*Theoretical Division and Center for Nonlinear Studies,*
*Los Alamos National Laboratory, Los Alamos, New Mexico 87545, USA*
(Dated: May 6, 2016)

Using a particle-based simulation model, we show that quenched disorder creates a drive-dependent skyrmion Hall effect as measured by the change in the ratio $R = V_\perp/V_{||}$ of the skyrmion velocity perpendicular ($V_\perp$) and parallel ($V_{||}$) to an external drive. $R$ is zero at depinning and increases linearly with increasing drive, in agreement with recent experimental observations. At sufficiently high drives where the skyrmions enter a free flow regime, $R$ saturates to the disorder-free limit. This behavior is robust for a wide range of disorder strengths and intrinsic Hall angle values, and occurs whenever plastic flow is present. For systems with small intrinsic Hall angles, we find that the Hall angle increases linearly with external drive, as also observed in experiment. In the weak pinning regime where the skyrmion lattice depins elastically, $R$ is nonlinear and the net direction of the skyrmion lattice motion can rotate as a function of external drive.

PACS numbers: 75.70.Kw,75.25.-j,75.47.Np

Skyrmions in magnetic systems are particle-like objects predicted to occur in systems with chiral interactions [1]. The existence of a hexagonal skyrmion lattice in chiral magnets was subsequently confirmed in neutron scattering experiments [2] and in direct imaging experiments [3]. Since then, skyrmion states have been found in an increasing number of compounds [4–8], including materials where skyrmions are stable at room temperature [9–13]. Skyrmions can be set into motion by applying an external current [14, 15], and effective skyrmion velocity versus driving force curves can be calculated from changes in the Hall resistance [16, 17] or by direct imaging of the skyrmion motion [9, 13]. Additionally, transport curves can be studied numerically with continuum and particle based models [18–22]. Both experiments and simulations show that there is a finite depinning threshold for skyrmion motion similar to that found for the depinning of current-driven vortex lattices in type-II superconductors [23–25]. Since skyrmions have particle like properties and can be moved with very low driving currents, they are promising candidates for spintronic applications [26, 27], so an understanding of skyrmion motion and depinning is of paramount importance. Additionally, skyrmions represent an interesting dynamical system to study due to the strong non-dissipative effect of the Magnus force they experience, which is generally very weak or absent altogether in other systems where depinning and sliding phenomena occur.

For particle-based representations of the motion of objects such as superconducting vortices, a damping term of strength $\alpha_d$ aligns the particle velocity in the direction of the net force acting on the particle, while a Magnus term of strength $\alpha_m$ rotates the velocity component in the direction perpendicular to the net force. In most systems studied to date, the Magnus term is very weak compared to the damping term, but in skyrmion systems the ratio of the Magnus and damping terms can be as large as $\alpha_m/\alpha_d \sim 10$ [16, 18, 20, 28]. One consequence of the dominance of the Magnus term is that under an external driving force, skyrmions develop velocity components both parallel ($V_{||}$) and perpendicular ($V_\perp$) to the external drive, producing a skyrmion Hall angle of $\theta_{sk} = \tan^{-1}(R)$, where $R = |V_\perp/V_{||}|$. In a completely pin-free system, the intrinsic skyrmion Hall angle has a constant value $\theta_{sk}^{\rm int} = \tan^{-1}(\alpha_m/\alpha_d)$; however, in the presence of pinning a moving skyrmion exhibits a side jump phenomenon in the direction of the drive so that the measured Hall angle is smaller than the clean value [21, 22, 29]. In studies of these side jumps using both continuum and particle based models for a skyrmion interacting with a single pinning site [21] and a periodic array of pinning sites [29], $R$ increases with increasing external drive until the skyrmions are moving fast enough that the pinning becomes ineffective and the side jump effect is reduced.

In particle-based studies of skyrmions with an intrinsic Hall angle of $\theta_{sk}^{\rm int} = 84^\circ$ moving through random pinning arrays, $\theta_{sk} = 40^\circ$ at small drives and increases with increasing drive until saturating at $\theta_{sk} = \theta_{sk}^{\rm int}$ at higher drives [22]. In recent imaging experiments [30] it was shown that $R = 0$ and $\theta_{sk} = 0$ at depinning and both increase linearly with increasing drive; however, the range of accessible driving forces was too low to permit observation of a saturation effect. These experiments were performed in a regime of relatively strong pinning, where upper limits of $R \sim 0.4$ and $\theta_{sk} = 20^\circ$ are expected. A natural question is how universal the linear behavior of $R$ and $\theta_{sk}$ as a function of drive is, and whether the results remain robust for larger intrinsic values of $\theta_{sk}$. It is also interesting to ask what happens in the weak pinning limit where the skyrmions form a hexagonal lattice and depin elastically. In studies of overdamped systems such as superconducting vortices, it is known that the strong and weak pinning limits are separated by a transition from elastic to plastic depinning and have very different transport curve characteristics [23, 25], so a similar phe-

nomenon could arise in the skyrmion Hall effect.

*Simulation and System*— We consider a 2D simulation with periodic boundary conditions in the $x$ and $y$-directions using a particle-based model of a modified Thiele equation recently developed for skyrmions interacting with random [20, 22] and periodic [29, 31] pinning substrates. The simulated region contains $N$ skyrmions, and the time evolution of a single skyrmion $i$ is governed by the following equation:

$$\alpha_d \mathbf{v}_i + \alpha_m \hat{\mathbf{z}} \times \mathbf{v}_i = \mathbf{F}_i^{ss} + \mathbf{F}_i^{sp} + \mathbf{F}^D. \quad (1)$$

Here, the skyrmion velocity is $\mathbf{v}_i = d\mathbf{r}_i/dt$, $\alpha_d$ is the damping term, and $\alpha_m$ is the Magnus term. We impose the condition $\alpha_d^2 + \alpha_m^2 = 1$ to maintain a constant magnitude of the skyrmion velocity for varied $\alpha_m/\alpha_d$. The repulsive skyrmion-skyrmion interaction force is given by $\mathbf{F}_i^{ss} = \sum_{j=1}^{N} \hat{\mathbf{r}}_{ij} K_1(r_{ij})$ where $r_{ij} = |\mathbf{r}_i - \mathbf{r}_j|$, $\hat{\mathbf{r}}_{ij} = (\mathbf{r}_i - \mathbf{r}_j)/r_{ij}$, and $K_1$ is the modified Bessel function which falls off exponentially for large $r_{ij}$. The pinning force $\mathbf{F}_i^{sp}$ arises from non-overlapping randomly placed pinning sites modeled as harmonic traps with an amplitude of $F_p$ and a radius of $R_p = 0.3$ as used in previous studies [22]. The driving force $\mathbf{F}^D = F_D\hat{\mathbf{x}}$ is from an applied current interacting with the emergent magnetic flux carried by the skyrmion [16, 28]. We increase $\mathbf{F}^D$ slowly to avoid transient effects. In order to match the experiments, we take the driving force to be in the positive $x$-direction so that the Hall effect is in the negative $y$-direction. We measure the average skyrmion velocity $V_{||} = \langle N^{-1} \sum_i^N \mathbf{v}_i \cdot \hat{\mathbf{x}} \rangle$ ($V_\perp = \langle N^{-1} \sum_i^N \mathbf{v}_i \cdot \hat{\mathbf{y}} \rangle$) in the direction parallel (perpendicular) to the applied drive, and we characterize the Hall effect by measuring $R = |V_\perp/V_{||}|$ for varied $F^D$. The skyrmion Hall angle is $\theta_{sk} = \tan^{-1} R$. We consider a system of size $L = 36$ with a fixed skyrmion density of $\rho_{sk} = 0.16$ and pinning densities ranging from $n_p = 0.00625$ to $n_p = 0.2$.

*Results and Discussion*— In Fig. 1(a,b) we plot $|V_\perp|$, $|V_{||}|$, and $R$ versus $F_D$ for a system with $F_p = 1.0$, $n_p = 0.1$, and $\alpha_m/\alpha_d = 5.708$. In this regime, plastic depinning occurs, meaning that at the depinning threshold some skyrmions can be temporarily trapped at pinning sites while other skyrmions move around them. The velocity-force curves are nonlinear, and $|V_\perp|$ increases more rapidly with increasing $F_D$ than $|V_{||}|$. The inset of Fig. 1(a) shows that $|V_{||}| > |V_\perp|$ for $F_D < 0.1$, indicating that just above the depinning transition the skyrmions are moving predominantly in the direction of the driving force. In Fig. 1(b), $R$ increases linearly with increasing $F_D$ for $0.04 < F_D < 0.74$, as indicated by the linear fit, while for $F_D > 0.74$ $R$ saturates to the intrinsic value of $R = 5.708$ marked with a dashed line. The inset of Fig. 1(b) shows the corresponding $\theta_{sk}$ vs $F_D$. Initially $\theta_{sk} = 0°$, but $\theta_{sk}$ increases with increasing $F_D$ before saturating at the clean limit value of $\theta_{sk} = 80.06°$. Although the linear increase in $R$ with $F_D$ is similar to the behavior observed in the experiments of Ref. [30],

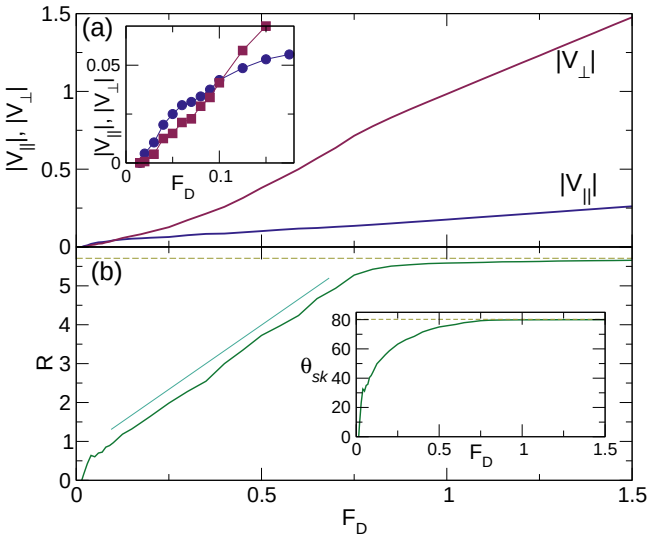


FIG. 1: (a) The skyrmion velocities in the directions parallel ($|V_{||}|$, blue) and perpendicular ($|V_\perp|$, red) to the driving force vs $F_D$ in a system with $\alpha_m/\alpha_d = 5.71$, $F_p = 1.0$, and $n_p = 0.1$. The drive is applied in the $x$-direction. Inset: a blowup of the main panel in the region just above depinning where there is a crossing of the velocity-force curves. (b) The corresponding $R = |V_\perp/V_{||}|$ vs $F_D$. The solid straight line is a linear fit and the dashed line is the clean limit value of $R = 5.708$. Inset: $\theta_{sk} = \tan^{-1}(R)$ vs $F_D$. The dashed line is the clean limit value of $\theta_{sk} = 80.06°$.

$\theta_{sk}$ does not show the same linear behavior as in the experiments; however, we show later that when the intrinsic skyrmion Hall angle is small, $\theta_{sk}$ varies linearly with drive.

In Fig. 2 we illustrate the skyrmion positions and trajectories obtained during a fixed period of time at different drives for the system in Fig. 1. At $F_D = 0.02$ in Fig. 2(a), $R = 0.15$ and the average drift is predominantly along the $x$-direction parallel to the drive, taking the form of riverlike channels along which individual skyrmions intermittently switch between pinned and moving states. In Fig. 2(b), for $F_D = 0.05$ we find $R = 0.6$, and observe wider channels that begin to tilt along the negative $y$-direction. At $F_D = 0.2$ in Fig. 2(c), $R = 1.64$ and $\theta_{sk} = 58.6°$. The skyrmion trajectories are more strongly tilted along the $-y$ direction, and there are still regions of temporarily pinned skyrmions coexisting with moving skyrmions. As the drive increases, individual skyrmions spend less time in the pinned state. Figure 2(d) shows a snapshot of the trajectories over a shorter time scale at $F_D = 1.05$ where $R = 5.59$. Here the plastic motion is lost and the skyrmions form a moving crystal translating at an angle of $-79.8°$ with respect to the external driving direction, which is close to the clean value limit of $\theta_{sk}$. In general, the deviations from linear behavior that appear as $R$ reaches its saturation value in Fig. 1(b) coincide with the loss of coexisting pinned and

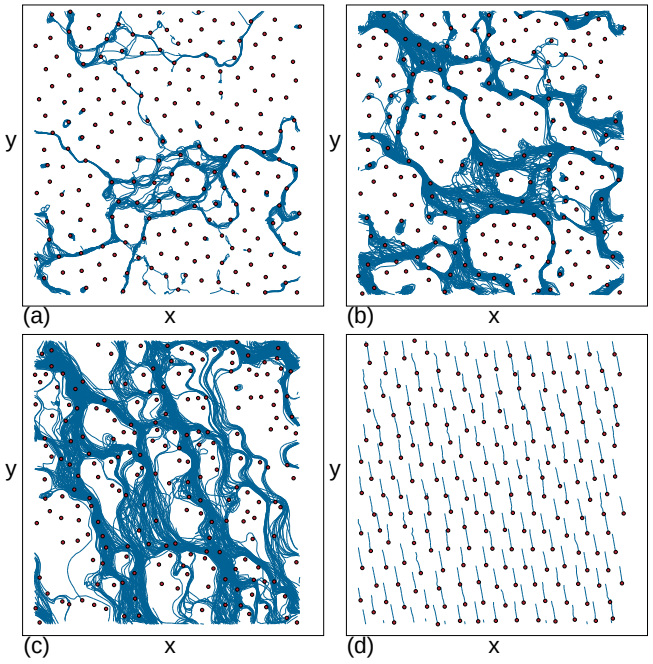


FIG. 2: Skyrmion positions (dots) and trajectories (lines) obtained over a fixed time period from the system in Fig. 1(a). The drive is in the positive $x$-direction. (a) At $F_D = 0.02$, $R = 0.15$ and the motion is mostly along the $x$ direction. (b) At $F_D = 0.05$, $R = 0.6$ and the flow channels begin tilting into the $-y$ direction. (c) At $F_D = 0.2$, $R = 1.64$ and the channels tilt further toward the $-y$ direction. (d) Trajectories obtained over a shorter time period at $F_D = 1.05$ where $R = 5.59$. The skyrmions are dynamically ordered and move at an angle of $-79.8^\circ$ to the drive.

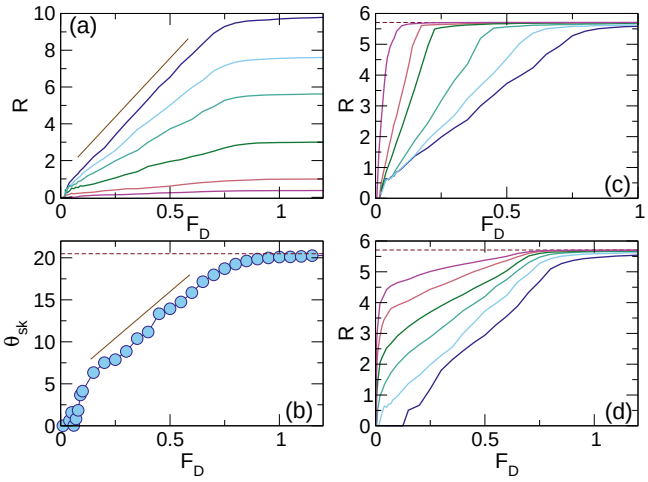


FIG. 3: (a) $R$ vs $F_D$ for samples with $F_p = 1.0$ and $n_p = 0.1$ at $\alpha_m/\alpha_d = 9.962$, 7.7367, 5.708, 3.042, 1.00, and 0.3737, from left to right. The line indicates a linear fit. (b) $\theta_{sk} = \tan^{-1}(R)$ for $\alpha_m/\alpha_d = 0.3737$ from panel (a). The solid line is a linear fit and the dashed line indicates the clean limit value of $\theta_{sk} = 20.5^\circ$. (c) $R$ vs $F_D$ for $\alpha_m/\alpha_d = 5.708$ at $F_p = 0.06125$, 0.125, 0.25, 0.5, 0.75, and 1.0, from left to right. (d) $R$ vs $F_D$ for $F_p = 1.0$ at $\alpha_m/\alpha_d = 5.708$ for $n_p = 0.00617$, 0.01234, 0.02469, 0.04938, 0.1, and 0.2, from left to right. The clean limit value of $R$ is indicated by the dashed line.

moving skyrmions, and are thus correlated with the end of plastic flow.

In Fig. 3(a) we show $R$ versus $F_D$ for the system from Fig. 1 at varied $\alpha_m/\alpha_d$. In all cases, between the depinning transition and the free flowing phase there is a plastic flow phase in which $R$ increases linearly with $F_D$ with a slope that increases with increasing $\alpha_m/\alpha_d$. In contrast to the nonlinear dependence of $\theta_{sk}$ on $F_D$ at $\alpha_m/\alpha_d = 5.71$ illustrated in the inset of Fig. 1(b), Fig. 3(b) shows that for $\alpha_m/\alpha_d = 0.3737$, $\theta_{sk}$ increases linearly with $F_D$, in agreement with the experiments of Ref. [30]. Here, $\theta_{sk}^{\rm int} = 20.5$, close to the value predicted in the experiments of Ref. [30]. To understand the linear behavior, consider the expansion of $\tan^{-1}(x) = x - x^3/3 + x^5/5...$ For small $\alpha_m/\alpha_d$, as in the experiments, $\tan^{-1}(R) \sim R$, and since $R$ increases linearly with $F_D$, $\theta_{sk}$ also increases linearly with $F_D$. In general, for $\alpha_m/\alpha_d < 1.0$ we find an extended region over which $\theta_{sk}$ grows linearly with $F_D$, while for $\alpha_m/\alpha_d > 1.0$, the dependence of $\theta_{sk}$ on $F_D$ has nonlinear features similar to those shown in the inset of Fig. 1(b). In Fig. 3(c) we plot $R$ versus $F_D$ for a system with $\alpha_m/\alpha_d = 5.708$ for varied $F_p$. In all cases $R$ increases linearly with $F_D$ before saturating; however, for increasing $F_p$, the slope of $R$ decreases while the saturation of $R$ shifts to higher values of $F_D$. In general, the linear behavior in $R$ is present whenever $F_p$ is strong enough to produce plastic flow. In Fig. 3(d) we show $R$ versus $F_D$ at $\alpha_m/\alpha_d = 5.708$ for varied pinning densities $n_p$. In each case, there is a region in which $R$ increases linearly with $F_D$, with a slope that increases with increasing $n_p$. As $n_p$ becomes small, the nonlinear region just above depinning where $R$ increases very rapidly with becomes more prominent.

For weak pinning, the skyrmions form a triangular lattice and exhibit elastic depinning, in which each skyrmion maintains the same neighbors over time. In Fig. 4(a) we plot the critical depinning force $F_c$ and the fraction $P_6$ of sixfold-coordinated skyrmions versus $F_p$ for a system with $n_p = 0.1$ and $\alpha_m/\alpha_d = 5.708$. For $0 < F_p < 0.04$, the skyrmions depin elastically. In this regime, $P_6 = 1.0$ and $F_c$ increases as $F_c \propto F_p^2$ as expected for the collective depinning of elastic lattices [24]. For $F_p \geq 0.04$, $P_6$ drops due to the appearance of topological defects in the lattice, and the system depins plastically, with $F_c \propto F_p$ as expected for single particle depinning or plastic flow.

In Fig. 4(b) we plot $R$ versus $F_D$ in samples with $F_p = 0.01$ in the elastic depinning regime for varied $\alpha_m/\alpha_d$. We highlight the nonlinear behavior for the $\alpha_m/\alpha_d = 5.708$ case by a fit of the form $R \propto (F_D - F_c)^\beta$ with $\beta = 0.26$ and $F_c = 0.000184$. The dotted line indicates the corresponding clean limit value of $R = 5.708$. We find that $R$ is always nonlinear within the elastic flow

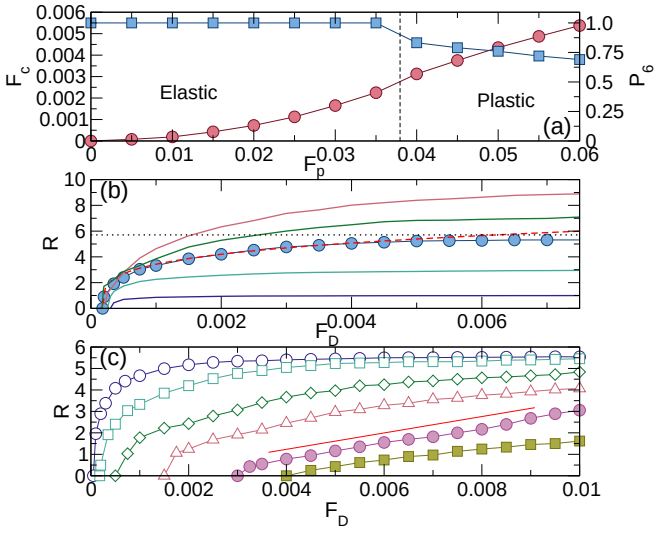


FIG. 4: (a) Depinning force $F_c$ (circles) and fraction $P_6$ of six-fold coordinated particles (squares) vs $F_p$ for a system with $\alpha_m/\alpha_d = 5.708$ and $n_p = 0.1$, showing a crossover from elastic depinning for $F_p < 0.04$ to plastic depinning for $F_p \geq 0.04$. (b) $R$ vs $F_D$ for a system in the elastic depinning regime with $F_p = 0.01$ and $n_p = 0.1$ at $\alpha_m/\alpha_d = 9.962$, 5.708, 3.042, and 1.00, from top to bottom. Circles indicate the case $\alpha_m/\alpha_d = 5.708$, for which the dashed line is a fit to $R \propto (F_D - F_c)^\beta$ with $\beta = 0.26$ and the dotted line indicates the pin-free value of $R = 5.708$. (c) $R$ vs $F_D$ for samples with $\alpha_m/\alpha_d = 5.708$ at $F_p = 0.005$, 0.01, 0.02, 0.03, 0.04, and 0.05, from left to right. The solid symbols correspond to values of $F_p$ for which plastic flow occurs, while open symbols indicate elastic flow. The line shows a linear dependence of $R$ on $F_D$ for $F_p = 0.04$.

regime, but that there is no universal value of $\beta$, which ranges from $\beta = 0.15$ to $\beta = 0.5$ with varying $\alpha_m/\alpha_d$. The change in the Hall angle with drive is most pronounced just above the depinning threshold, as indicated by the rapid change in $R$ at small $F_D$. This results from the elastic stiffness of the skyrmion lattice which prevents individual skyrmions from occupying the most favorable substrate locations. In contrast, $R$ changes more slowly at small $F_D$ in the plastic flow regime, where the softer skyrmion lattice can adapt to the disordered pinning sites. In Fig. 4(c) we plot $R$ versus $F_D$ at $\alpha_m/\alpha_d = 5.708$ for varied $F_p$, showing a reduction in $R$ with increasing $F_p$. A fit of the $F_p = 0.04$ curve in the plastic depinning regime shows a linear increase of $R$ with $F_D$, while for $F_p < 0.04$ in the elastic regime, the dependence of $R$ on $F_D$ is nonlinear. Just above depinning in the elastic regime, the skyrmion flow direction rotates with increasing drive.

*Summary*— We have investigated the skyrmion Hall effect by measuring the ratio $R$ of the skyrmion velocity perpendicular and parallel to an applied driving force. In the disorder-free limit, $R$ and the skyrmion Hall angle take constant values independent of the applied drive; however, in the presence of pinning these quantities become drive-dependent, and in the strong pinning regime $R$ increases linearly from zero with increasing drive, in agreement with recent experiments. For large intrinsic Hall angles, the current-dependent Hall angle increases nonlinearly with increasing drive; however, for small intrinsic Hall angles such as in recent experiments, both the current-dependent Hall angle and $R$ increase linearly with drive as found experimentally. The linear dependence of $R$ on drive is robust for a wide range of intrinsic Hall angle values, pinning strengths, and pinning densities, and appears whenever the system exhibits plastic flow. For weaker pinning forces where the skyrmions depin elastically, $R$ has a nonlinear drive dependence and increases very rapidly just above depinning. We observe a crossover from nonlinear to linear drive dependence of $R$ as a function of the pinning force, which coincides with the transition from elastic to plastic depinning.

We gratefully acknowledge the support of the U.S. Department of Energy through the LANL/LDRD program for this work. This work was carried out under the auspices of the NNSA of the U.S. DoE at LANL under Contract No. DE-AC52-06NA25396.

[1] U.K. Rößler, A.N. Bogdanov, and C. Pfleiderer, Nature (London) **442**, 797 (2006).
[2] S. Mühlbauer, B. Binz, F. Jonietz, C. Pfleiderer, A. Rosch, A. Neubauer, R. Georgii, and P. Böni, Science **323**, 915 (2009).
[3] X.Z. Yu, Y. Onose, N. Kanazawa, J.H. Park, J.H. Han, Y. Matsui, N. Nagaosa, and Y. Tokura, Nature (London) **465**, 901 (2010).
[4] S. Heinze, K. von Bergmann, M. Menzel, J. Brede, A. Kubetzka, R. Wiesendanger, G. Bihlmayer, and S. Blulgel, Nature Phys. **7**, 713 (2011).
[5] X.Z. Yu, N. Kanazawa, Y. Onose, K. Kimoto, W.Z. Zhang, S. Ishiwata, Y. Matsui, and Y. Tokura, Nature Mater. **10**, 106 (2011).
[6] S. Seiki, X.Z. Yu, S. Ishiwata, and Y. Tokura, Science **336**, 198 (2012).
[7] K. Shibata, X.Z. Yu, T. Hara, D. Morikawa, N. Kanazawa, K. Kimoto, S. Ishiwata, Y. Matsui, and Y. Tokura, Nature Nanotechnol. **8**, 723 (2013).
[8] I. Kézsmárki, Nature Mater. **14**, 1116 (2015)
[9] W. Jiang, P. Upadhyaya, W. Zhang, G. Yu, M. B. Jungfleisch, F. Y. Fradin, J. E. Pearson, Y. Tserkovnyak, K. L. Wang, O. Heinonen, S. G. E. te Velthuis, and A. Hoffmann, Science **349**, 283 (2015).
[10] G. Chen, A. Mascaraque, A.T. N'Diaye, and A.K. Schmid, Appl. Phys. Lett. **106**, 242404 (2015).
[11] Y. Tokunaga, X. Z. Yu, J. S. White, H. M. Rønnow, D. Morikawa, Y. Taguchi, and Y. Tokura, Nature Commun. **6**, 7638 (2015).
[12] O. Boulle, J. Vogel, H. Yang, S. Pizzini, D. de Souza Chaves, A. Locatelli, T.O. Mentes, A. Sala, L.D. Buda-Prejbeanu, O. Klein, M. Belmeguenai, Y. Roussigné, A. Stashkevich, S.M. Chérif, L. Aballe, M. Foerster, M.

Chshiev, S. Auffret, I.M. Miron, and G. Gaudin, Nature Nanotechnol., in press (2016).
[13] S. Woo, K. Litzius, B. Krüger, M. Im, L. Caretta, K. Richter, M. Mann, A. Krone, R. Reeve, M. Weigand, P. Agrawal, I. Lemesh, M. Mawass, P. Fischer, M. Kläui, and G. Beach, Nature Mater. **15**, 501 (2016).
[14] F. Jonietz, S. Mühlbauer, C. Pfleiderer, A. Neubauer, W. Münzer, A. Bauer, T. Adams, R. Georgii, P. Böni, R.A. Duine, K. Everschor, M. Garst, and A. Rosch, Science **330**, 1648 (2010).
[15] X.Z. Yu, N. Kanazawa, W.Z. Zhang, T. Nagai, T. Hara, K. Kimoto, Y. Matsui, Y. Onose, and Y. Tokura, Nature Commun. **3**, 988 (2012).
[16] T. Schulz, R. Ritz, A. Bauer, M. Halder, M. Wagner, C. Franz, C. Pfleiderer, K. Everschor, M. Garst, and A. Rosch, Nature Phys. **8**, 301 (2012).
[17] D. Liang, J.P. DeGrave, M.J. Stolt, Y. Tokura, and S. Jin, Nature Commun. **6**, 8217 (2015).
[18] J. Iwasaki, M. Mochizuki, and N. Nagaosa, Nature Commun. **4**, 1463 (2013).
[19] J. Iwasaki, M. Mochizuki, and N. Nagaosa, Nature Nanotechnol. **8**, 742 (2013).
[20] S.-Z. Lin, C. Reichhardt, C.D. Batista, and A. Saxena, Phys. Rev. B **87**, 214419 (2013).
[21] J. Müller and A. Rosch, Phys. Rev. B **91**, 054410 (2015).
[22] C. Reichhardt, D. Ray, and C.J. Olson Reichhardt, Phys. Rev. Lett. **114**, 217202 (2015).
[23] S. Bhattacharya and M.J. Higgins, Phys. Rev. Lett. **70**, 2617 (1993).
[24] G. Blatter, M.V. Feigelman, V.B. Geshkenbein, A.I. Larkin, and V.M. Vinokur, Rev. Mod. Phys. **66**, 1125 (1994).
[25] C.J. Olson, C. Reichhardt, and F. Nori, Phys. Rev. Lett. **81**, 3757 (1998).
[26] A. Fert, V. Cros, and J. Sampaio, Nature Nanotechnol. **8**, 152 (2013).
[27] R. Tomasello, E. Martinez, R. Zivieri, L. Torres, M. Carpentieri, and G. Finocchio, Sci. Rep. **4**, 6784 (2014).
[28] N. Nagaosa and Y. Tokura, Nature Nanotech. **8**, 899 (2013).
[29] C. Reichhardt, D. Ray, and C. J. Olson Reichhardt, Phys. Rev. B **91**, 104426 (2015).
[30] W. Jiang, X. Zhang, G. Yu, W. Zhang, M.B. Jungfleisch, J.E. Pearson, O. Heinonen, K.L. Wang, Y. Zhou, A. Hoffmann, and S.G.E. te Velthuis, arXiv:1603.07393 (unpublished).
[31] C. Reichhardt and C. J. Olson Reichhardt, Phys. Rev. B **92**, 224432 (2015)